

Rachel E. Jordan<sup>1\*</sup>, Edgar L. Andreas<sup>1</sup>, Christopher W. Fairall<sup>2</sup>, Andrey A. Grachev<sup>3</sup>, Peter S. Guest<sup>4</sup>,  
John M. Hanesiak<sup>5</sup>, Donald K. Perovich<sup>1</sup>, and P. Ola G. Persson<sup>3</sup>

<sup>1</sup>U.S. Army Cold Regions Research and Engineering Laboratory, Hanover, New Hampshire

<sup>2</sup>NOAA Environmental Technology Laboratory, Boulder, Colorado

<sup>3</sup>Cooperative Institute for Research in Environmental Sciences, University of Colorado, Boulder, Colorado

<sup>4</sup>Naval Postgraduate School, Monterey, California

<sup>5</sup>Centre for Earth Observation Science, University of Manitoba, Winnipeg, Manitoba, Canada

## 1. INTRODUCTION

The snow cover on sea ice acts as an insulator against frigid Arctic air and inhibits wintertime ice growth at the ocean interface. It has an especially disproportionate effect in the fall, when snow is less dense, and even a shallow cover can dramatically slow cooling of the sea ice. We use a detailed, one-dimensional model of snow, SNTHERM, to simulate heat exchange within and at the surface of the shallow snow cover at the SHEBA (Surface Heat Budget of the Arctic Ocean) ice camp. Although SNTHERM was developed originally for snow-covered ground, we recently adapted it to also handle snow-covered sea ice. We have tested a polar version, SNTHERMP, with data from Russian drifting station North Pole 4 (NP-4) and from Ice Station Weddell (ISW). Extensive year-long measurements from SHEBA provide data for further testing our model and for investigating the thermal regime within this shallow snowpack. Here we limit our investigation to the first snow season at SHEBA.

We validate in-snow thermal processes by comparing simulated temperature traces and profiles with thermistor readings at five levels within the snow cover. Overall, it was difficult to simulate sufficient cooling of the SHEBA snowpack, particularly during the early winter. Possible reasons for this discrepancy could be that SNTHERMP underpredicts snow density or thermal conductivity or that it omits heat transfer processes other than conduction.

We estimate turbulent fluxes at the snow surface with a routine recently developed for ISW. This

includes a new parameterization for the roughness length  $z_0$  and a variable von Kármán “constant.” Simulated momentum and heat fluxes correlate well with approximately 3,500 hours of eddy-correlation measurements. Simulated time series of surface temperatures match radiometric observations to within 1°C, thus corroborating the correctness of our surface flux simulation.

Because detailed snow models are not practical for global climate models (GCMs), it is instructive to examine the accuracy of simpler snow treatments. We therefore present two alternate SNTHERMP simulations of turbulent exchange. In the first, we assume a snowpack that is homogeneous in density and thermal conductivity but has multiple layers, each with a unique temperature; in the second, we additionally limit the model to just one snow layer.

## 2. MODEL

### 2.1 Model overview

SNTHERM simulates most snow cover properties and processes, including heat conduction, phase change, water flow, snow ablation and accumulation, densification, grain growth, subsurface absorption of solar radiation, and surface energy exchange. The snow cover is modeled numerically as a one-dimensional, layered mixture of dry air, ice, liquid water, and water vapor. SNTHERM uses a control volume scheme with a moving mesh that compresses over time as the snow compacts. Control volumes are added at the start of snowfall events or when the accumulating snow reaches 4 cm depth and thus coincide with the natural stratigraphy of the snow cover.

SNTHERM models only thermal processes for soil layers and therefore includes a sink that artificially drains infiltrating water when it reaches

---

\*Corresponding author address: Rachel E. Jordan, U.S. Army Cold Regions Research and Engineering Lab, 72 Lyme Road, Hanover, NH 03755-1290; e-mail: rjordan@crrel.usace.army.mil.

the soil–snow interface (Jordan 1991). Rowe et al. (1995) simulated snowmelt on the Greenland ice sheet using a modified version of SNTHERM that replaces the underlying ground layer with ice. Their procedure makes advantageous use of the intralayer drain and avoids problems of ponding water, which are not handled in SNTHERM. We treat the sea ice layer in a similar fashion but additionally consider the effect of salinity on the thermal properties.

Jordan et al. (1999) describe modifications we made to SNTHERM to model the snow cover and sea ice at Russian drifting station North Pole 4. Strong winds, the cold, and the sea ice substrate necessitated all these changes. Jordan et al. (2001) and Andreas et al. (2003b) describe further adaptations made to accommodate flooded sea ice during the four-month drift of Ice Station Weddell (ISW). Henceforth, we refer to the polar version of SNTHERM as SNTHERMP. Here we summarize the major polar features of SNTHERMP and discuss special modifications made for SHEABA. All units in what follows are MKS.

## 2.2 Thermal properties

Following Maykut and Untersteiner (1971; henceforth MU), we parameterize the thermal properties of sea ice in terms of its temperature depression  $T_D$  below  $0^\circ\text{C}$  and its bulk salinity  $S$ . We modify their thermal conductivity function to account for the air content of ice. Following Schwerdtfeger (1963), we use a Maxwell-type expression for the resistivity of a compound medium containing uniformly distributed spherical bubbles of air. Latent heat effects in MU's apparent heat capacity expression are expressed in terms of a thermodynamically based freezing curve that can also extend to snow (Andreas et al. 2003b).

Process-based snow models primarily estimate thermal conductivity  $k_s$  from snow density and secondarily from temperature. Because crystal shape and bond geometry are not considered, measurements grouped by density show considerable scatter. Hence, functions based on density alone are not that reliable. Figure 1, for instance, shows differences of almost a factor of 2 between Yen's (1965) laboratory measurements on old snow and extensive field measurements on high-latitude snow by Sturm et al. (1997). Summary articles on thermal conductivity (e.g., Sturm et al., 1997) confirm the large scatter in both measure-

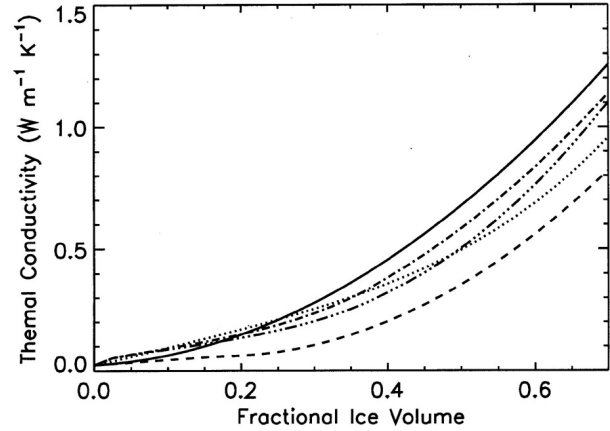


Fig. 1. Thermal conductivity as related to fractional ice volume from the parameterizations of Yen (1965)-Jordan (1991) at  $-20^\circ\text{C}$  (solid line), Morris et al. (1997) (dotted), Sturm et al. (1997) (dashed), modified Pitman and Zuckerman (1968) at  $-10^\circ\text{C}$  (dash dot), and modified Pitman and Zuckerman at  $-30^\circ\text{C}$  (dash dot dot dot). SNTHERMP used the Pitman and Zuckerman parameterization.

ments and functions. For comparison, we show a composite fit to the published data used by Morris et al. (1997) in the long-standing DAISY model, a European counterpart to SNTHERM.

SNTHERM has long used Yen's formula for predicting thermal conductivity. Because his function overpredicts  $k_s$  for the dense snow typical of polar regions, Andreas et al. (2003b) switched instead to a modified version (Crocker 1984) of the analytical model of Pitman and Zuckerman (PZ) (1968). The PZ model incorporates vapor diffusion in an effective conductivity  $k_g$  for the gas phase, which enhances the thermal conductivity of air in the snow mixture by 1.8 and 1.1 at respective temperatures of  $-5^\circ\text{C}$  and  $-27^\circ\text{C}$ . The model is extremely sensitive to  $k_g$ , and for the very low temperatures at SHEBA it predicted  $k_s$  well below the Morris composite curve. We therefore increased the unit bond area (a fitting parameter in the PZ model) from 0.0071 to 0.012.

## 2.3 Turbulent exchange

SNTHERM predicts the turbulent fluxes of sensible and latent heat flux ( $H_s$  and  $H_L$ ) with a bulk flux algorithm such that

$$H_s = [\rho_a c_p C_{\text{Hr}} U_r + E_o] (T_s - \Theta_r) \quad (1a)$$

$$H_L = \rho_a L_v C_{Er} U_r (Q_s - Q_r). \quad (1b)$$

Here,  $\rho_a$  is the air density;  $c_p$  is the specific heat of air at constant pressure;  $L_v$  is the latent heat of sublimation;  $U_r$ ,  $\Theta_r$ , and  $Q_r$  are hourly averaged values of the wind speed, potential temperature, and specific humidity at a reference height  $r$ , respectively;  $T_s$  and  $Q_s$  are the same quantities at the surface, where the latter is evaluated as the saturation value.  $E_0$  is a windless transfer coefficient ( $= 1.0 \text{ W m}^{-2} \text{ K}^{-1}$ ) that prevents decoupling of the snow surface from the atmosphere under extremely stable conditions (Jordan et al. 1999). The bulk transfer coefficients for sensible ( $C_{Hr}$ ) and latent ( $C_{Er}$ ) heat are computed from the roughness lengths  $z_0$ ,  $z_T$ , and  $z_Q$  for momentum, heat, and moisture as

$$C_{Hr} = \frac{k^2}{\left[ \ln(r/z_0) - \psi_m(r/L) \right] \left[ \ln(r/z_T) - \psi_h(r/L) \right]} \quad (2a)$$

$$C_{Er} = \frac{k^2}{\left[ \ln(r/z_0) - \psi_m(r/L) \right] \left[ \ln(r/z_Q) - \psi_h(r/L) \right]} \quad (2b)$$

Here  $k$  is the von Kármán constant, which we take as a variable following Andreas et al. (2002, 2003b). Also,  $\psi_m$  and  $\psi_h$  are known corrections to the wind speed and scalar profiles that account for stratification effects through the stability parameter  $r/L$ , where  $L$  is the Obukhov length. For unstable stratification (i.e.,  $\Theta_r < T_s$  and  $L < 0$ ), we use Paulson's (1970) functions. For stable stratification (i.e.,  $\Theta_r > T_s$  and  $L > 0$ ), we use the so-called "Dutch" formulation of Holtslag and DeBruin (1988) because these functions extend the region of turbulent exchange in very stable stratification (Jordan et al. 1999; Andreas 2002).

For  $z_0$  we use

$$z_0 = \frac{0.135\nu}{u_*} + 2.0 \times 10^{-4} \exp \left[ \left( \frac{u_* - 0.25}{0.15} \right)^2 \right] + \frac{0.030u_*^2}{g} \quad (3)$$

where  $\nu$  is the kinematic viscosity of air,  $u_*$  is the friction velocity, and  $g$  is the acceleration of gravity. Equation (3) is similar in form to functions that Jordan et al. (2001) and Andreas et al. (2003a) use to model  $z_0$  at ISW, but here the coefficients are fit to data from the SHEBA experiment (Andreas et al. 2003c). SNTHERM has long used

Andreas's (1987) theoretical model for the scalar roughness lengths  $z_T$  and  $z_Q$  (Jordan et al. 1999, Andreas et al. 2003a).

## 2.4 Wind effects

To handle drifting snow and ablation in windy polar regions, SNTHERMP computes a wind advection flux that can be "tuned" by adjusting the fractional stress gradient. Because SNTHERMP computes the threshold friction velocity from updated snow characteristics, it realistically predicts greater advection for newer, rather than older, snow. To the standard compaction routine, SNTHERMP adds a provisional wind-packing term that increases with wind transport and decreases exponentially with depth below the surface.

We further adapted SNTHERMP for SHEBA to include convective transport of heat through wind pumping. Surface microtopography, such as sastrugi or snow dunes, generate pressure perturbations that force air through the snow pack. Cunningham and Waddington (1993) compute the vertical velocity  $U_z$  of air pumped through snow as

$$U_z = \frac{K}{\pi^2 \mu \delta} P \exp^{-\frac{z}{\delta}} \quad (4)$$

Here  $K$  is the permeability of the snow cover ( $\text{m}^2$ ),  $\mu$  is the dynamic viscosity of air,  $P$  is the pressure perturbation (Pa),  $z$  is the depth below the snow surface (m), and  $\delta$  is the depth attenuation coefficient.  $\delta$  is related to a horizontal aspect ratio  $\alpha$  and a topographic wavelength  $\lambda$  as

$$\delta = \frac{\lambda}{2\pi} \frac{\alpha}{\sqrt{(\alpha^2 + 1)}} \quad (5)$$

and  $P$  relates to the 10-m wind speed as

$$P = C \rho_a \frac{H}{\lambda} U_{10}^2 \quad (6)$$

where  $H$  is the height of the topographic relief, and  $C$  is a fitting parameter. We select parameter values in the mid-range of Cunningham and Waddington's analysis:  $H = 0.15 \text{ m}$ ,  $\lambda = 2 \text{ m}$ ,  $\alpha = 1$ , and  $C = 3.0$ . The convective heat flux  $Q_w$  generated by wind pumping computes from  $U_z$  and the in-depth snow temperature at  $T_z$ :

$$Q_w = c_p \rho_a U_z T_z \quad (7)$$

## 2.5 New snow density

Because the cold polar snowpack does not compact rapidly, model results are very sensitive to the initial density of the deposited snow. For modeling new-snow density at Russian drifting station NP-4, Jordan et al. (1999) incorporated wind and temperature effects in a function that predicted densities between about 150 and 250 kg m<sup>-3</sup> for dry snow falling in windy conditions. This function worked well at SHEBA, except during cold, calm conditions, when simulated fresh snow was too light.

Very light snowfalls below 50 kg m<sup>-3</sup> are often composed of dendritic crystals that form when the air temperature is around -10°C (e.g., Colbeck et al. 1990). Above and below this general temperature, simpler shapes prevail and snow is more dense. For SHEBA, we modified our function to reach a minimum density of about 50 kg m<sup>-3</sup> at -10°C and then to increase with decreasing temperature up to a maximum density at -20°C. Simulated maximum densities at -20°C were 123, 168, and 247 kg m<sup>-3</sup> for respective wind speeds of 0, 5, and 10 m s<sup>-1</sup>. Kharitonov (1974) reports new-snow densities of around 110 kg m<sup>-3</sup> at -16°C and a general increase of density with decreasing temperature below about -12°C. We are unaware of other studies on this temperature dependence at low temperatures.

## 3. THE DATA

Our investigation simulates snow cover at the "Pittsburgh" thermistor string, which was located on a multiyear floe near the main SHEBA camp. Our study begins on 31 October 1997 (DOY 304) and ends on 14 July 1998 (DOY 195), a few days after the winter snow cover disappeared on 30 June (DOY 181).

We drive SNTHERMP with hourly averaged observations of air temperature, relative humidity, wind speed, incoming and outgoing solar radiation, and incoming longwave radiation from the Atmospheric Surface Flux Group (ASFG) site about 100 m from Pittsburgh (Andreas et al. 1999, Persson et al. 2002). This site was also on a multiyear floe and featured a 20-m tower that held five levels of eddy-correlation instruments. We use the measurements of sensible and latent heat fluxes from these for our comparisons later.

Because SNTHERMP does not predict ice accretion or ablation at the ice underside, we derive a lower boundary condition from thermistor readings at 180 cm depth in the ice.

SNTHERMP builds the snow cover with precipitation measurements provided by the SHEBA Project Office (SPO) (R. Moritz, personal communication, 2000; see [www.ofps.ucar.edu/codiac](http://www.ofps.ucar.edu/codiac)). Measurements were made with a Nipher-shielded snow gauge and were corrected for losses due to evaporation, gauge wetting, and wind according to the procedures of Goodison and Yang (1996). Even with these enhancements, accumulated precipitation was only 1/2 to 2/3 that on the ground (Sturm et al. 2002b). We therefore further increased precipitation by 50%, as recommended by the Sea-Ice Model Intercomparison (SIMIP2) website ([www.cccma.bc.ec.gc.ca/acsys/simip2/](http://www.cccma.bc.ec.gc.ca/acsys/simip2/)). Simulated snow depth then closely matched the observed maximum of approximately 45 cm.

There were, however, occasional false jumps in the simulated trace when snowfall coincided with blowing snow. In estimating precipitation at Russian drifting station NP-4, Jordan et al. (1999) adjusted the wind correction factor for the Tretyakov gauge to account for snow blowing into the gauge and registering as false precipitation. Here we use a similar approach and decrease the Goodison and Yang wind factor from a maximum enhancement of about 2 for a wind speeds of 8 m s<sup>-1</sup> to a 10-fold reduction for winds exceeding 20 m s<sup>-1</sup>. The most notable readjustment occurred for 26 January, when 18.6 mm of precipitation reduced to 6.2 mm.

Snow pit data, ice cores, and thermistor measurements provided initial values of snow density, salinity, and temperature at 21 levels within the snow and sea ice. At the start of our simulation, there were 10 cm of snow-ice (Sturm et al. 2002b), which we initialized as two snow layers with densities of 400 and 500 kg m<sup>-3</sup>. The ice salinity profile came from the SIMIP2 website and was provided by D. Perovich. Because no ice cores were done in the fall at SHEBA, this profile is from the spring. Ice density measurements were unavailable for Pittsburgh. We estimated density profiles as the average of the two multiyear ice stations provided on the SHEBA CD (Perovich et al. 1999). Perovich and Elder (2001) describe the thermistor strings and temperature measurements we use to both initialize and validate the model.

## 4. RESULTS

### 4.1 Snow accumulation

To correctly predict temperature profiles and assess SNTHERMP's ability to predict heat

transfer within the snowpack, we need to accurately simulate the observed snow depths at the thermistor location. Figure 2 compares snow depth from two simulations with two measured depths. The first are ablation stake measurements from the SIMIP2 website, and the second are depths inferred from the thermistor profiles. The ablation stake was collocated with thickness gauge 69, about 2 m from the thermistor string. Because the in-snow thermistors were spaced at 10-cm intervals, these profile estimates are accurate to about  $\pm 5$  cm. The marked differences in snow depth between these nearby locations highlight the extreme heterogeneity of the snow cover at wind-blown sites underlain with deformed ice. Sturm et al. (2002b) and Perovich et al. (2003) further discuss the spatial variability of the snow cover at SHEBA.

For simulation A, we used the precipitation provided by the SPO but increased by 50%. This produced the correct maximum snow cover and reasonably replicated depth at the ablation stake. In comparison to the thermistor location, however, the simulated fall and winter snow cover was too shallow.

For simulation B, we better replicated the thermistor depth by adding drifting and blowing snow for the first two months and eroding the snow cover in the spring. To do this, we assumed a fractional stress gradient of  $-0.007$  through 31 December 1997 (DOY 365) and a fractional stress gradient of  $0.008$  after 16 March 1998 (DOY 75). Blowing snow added 36 mm of snow water equivalent (SWE) to the snowpack through 31

December. In simulation B, we also reduced the precipitation correction factor for wind speeds over  $8 \text{ m s}^{-1}$ , as described above. This change decreased overall accumulation by about 20 mm of SWE.

Between 28 March and 11 May, Sturm et al. (2002b) made intensive measurements of snow characteristics at 70 locations in the vicinity of the SHEBA camp. We do a “spot-check” of our model by comparing observed and simulated characteristics at Pittsburgh for 2 April (DOY 92). Averages of snow depth, density, and SWE for 12 points along the Pittsburgh line were respectively 0.40 m,  $375 \text{ kg m}^{-3}$ , and 148 mm (Perovich et al., 1999). By comparison, simulation B produced 0.42 m depth,  $359 \text{ kg m}^{-3}$  density, and 150 mm SWE for 2 April.

Although simulated and observed average snow characteristics agree closely for 2 April, a comparison of density profiles shows some differences. Sturm et al. (2002b) distinguish 10 snow layers in the SHEBA snow cover (see their Fig. 3). The precipitation record contained about 30 snowfall events, most of which were represented by at least one layer in the SNTHERMP simulation. The thinner layers were not distinguished in the field by Sturm et al. A comparison of modeled and measured profiles for early May shows general similarities. SNTHERMP predicts the less-dense snow near the surface (layers “j” and “i” in Fig. 3 of Sturm et al. 2002b) and captures the higher density for the wind-blown snow of early December (layer “f”). High winds of late January and early March, however, simulate a drifted layer that is denser than observed layer “g.”

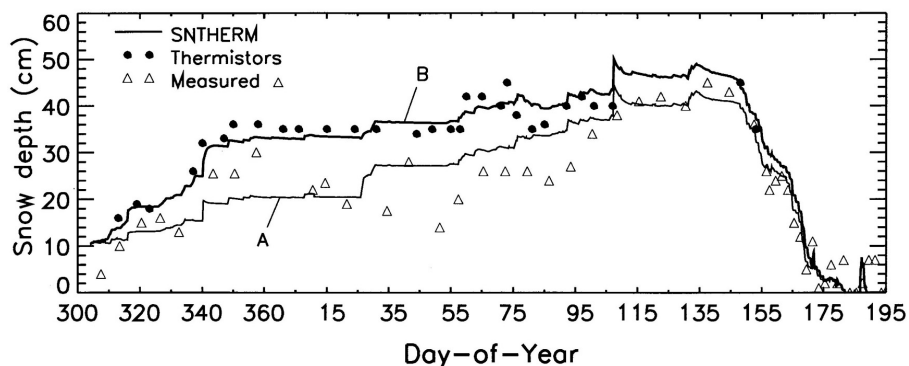


Fig. 2. Simulated snow depth between 31 October 1997 and 14 July 1998 at SHEBA. Simulation A uses precipitation provided by the SPO but increased by 50%. Simulation B advects snow before 1 January 1998 and ablates snow after 16 March 1998. Precipitation is the same as for A, except that the wind correction factor is reduced for wind speeds above  $8 \text{ m s}^{-1}$ . Measured snow depth (triangles) is from an ablation stake at the Pittsburgh site, and circles indicate depth inferred from the thermistor profiles.

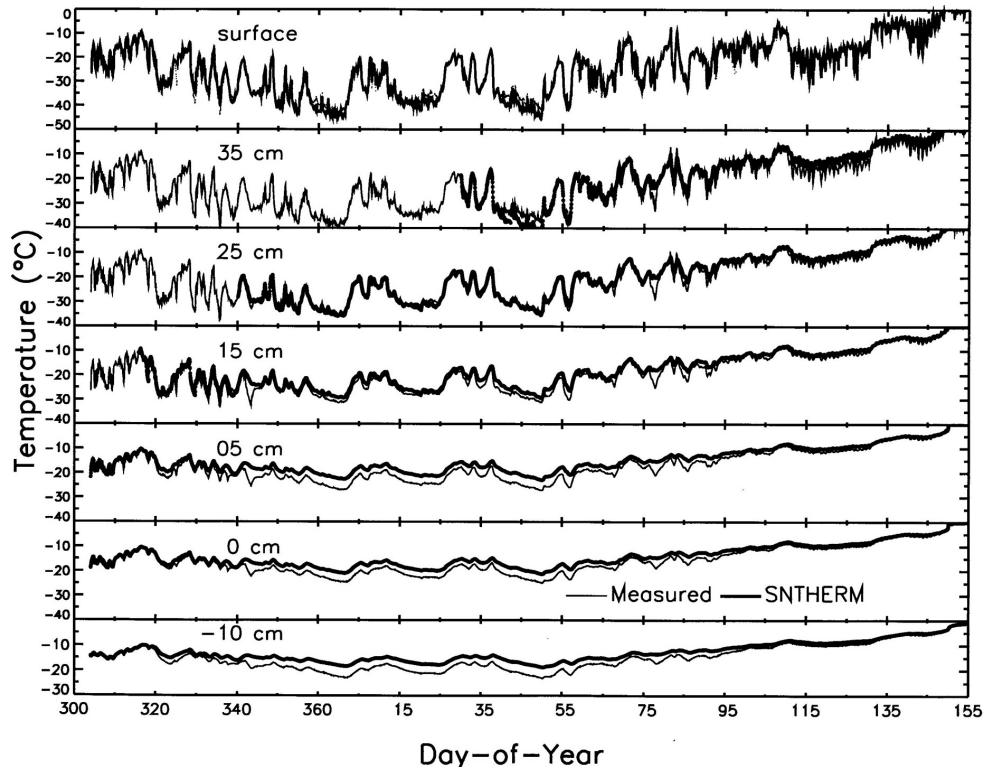


Fig. 3. Simulated (thick line) and measured (thin line) surface and in-snow temperature traces for the Pittsburgh site at SHEBA between 31 October 1997 and 4 June 1998. Dots indicate measured snow surface temperatures. Depth is measured relative to the snow-ice interface.

Simulated new-snow density of  $149 \text{ kg m}^{-3}$  for 1 April (DOY 91) compared favorably with an observed density of  $150 \text{ kg m}^{-3}$  for fresh snow at Pittsburgh, thus giving us at least one validation point for the revised low-temperature function. For the period of snowfall on 31 March (DOY 90), air temperatures and wind speeds were around  $-19^\circ\text{C}$  and  $8 \text{ m s}^{-1}$ .

#### 4.2 Heat transfer within the snow cover

Figure 3 compares measured and modeled temperature traces at the thermistor levels within the snow cover and at 10 cm depth within the sea ice. Considering the large temperature swings at the surface, SNThERM tracks the thermistor readings remarkably well. Predictions overall were too high near the ice surface and slightly too low near the snow surface during the coldest periods.

What causes overprediction of snow temperature at the ice interface? The cause must be either insufficient removal of heat due to cooling at the surface or a surplus of heat due to warming from the ocean. In the winter, heat

transfer through the ice is purely by conduction and is thus governed by its thermal conductivity  $k_i$ . Even though uncertainty in our ice properties caused an uncertainty in  $k_i$ , we do not sense that our estimated  $k_i$  for ice is too high.

Figure 3 suggests that the simulated  $k_s$  for the snow cover was too low. Indeed, an alternate simulation using a uniform value of  $0.33 \text{ W m}^{-1} \text{ K}^{-1}$  for  $k_s$  predicted snow-ice interfacial temperatures that were  $2^\circ\text{C}$  colder than the standard simulation during early winter. By late winter, however, modeled temperatures for both simulations were equally too high.

The only heat transfer mechanism SNThERM usually considers for dry snow is conduction. Because the simulated thermal conductivity for snow  $k_s$  was fairly high and because simulated traces do not track cooling beginning with a windy period around 3 December (DOY 337), we considered the additional possibility of heat transfer by windpumping. Natural convection (Sturm 1991) and horizontal heat transfer (Sturm et al. 2002a) are also possible in polar snowpacks with strong thermal gradients.

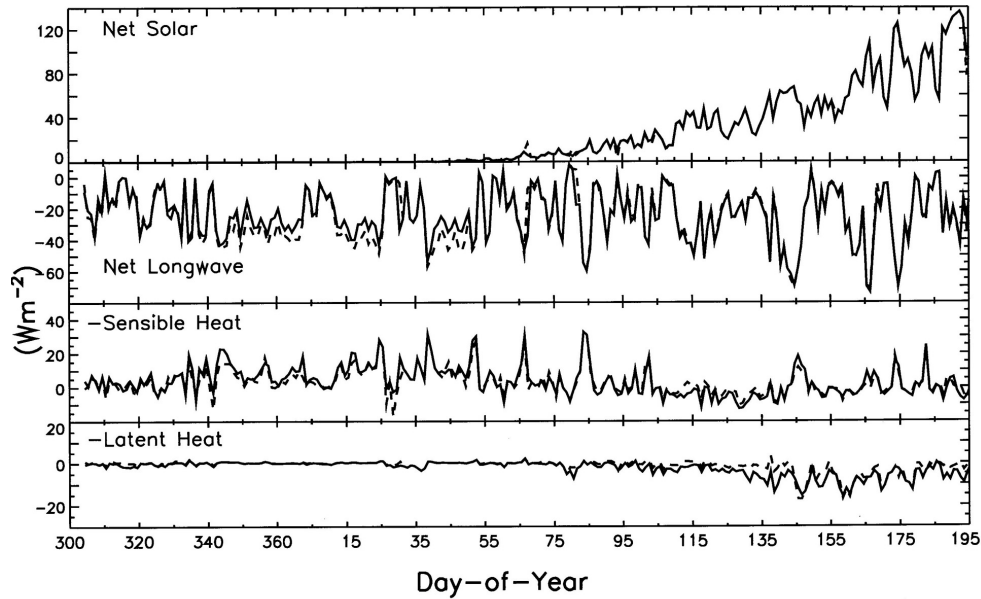


Fig. 4. Daily averages of modeled (solid line) and measured (dashed line) net shortwave radiation, net longwave radiation, and the negatives of the surface sensible and latent heat fluxes at SHEBA between 31 October 1997 and 14 July 1998. Measured values are from Persson et al. (2002).

Applying the windpumping procedure described above produced the proper cooling at the bottom of the snowpack and decreased the overall error for the entire run. For 6 December, winds up to  $15 \text{ m s}^{-1}$  caused vertical air velocities at the surface of  $4\text{--}7 \text{ mm s}^{-1}$  and at 20 cm depth of  $1\text{--}3 \text{ mm s}^{-1}$ . The net cooling to the snowpack for this period was on average  $5 \text{ W m}^{-2}$  greater than for conduction alone. Including windpumping, however, increased overcooling near the snow surface. For the most accurate surface flux prediction, we therefore use the standard SNTHERMP simulation.

Figure 3 shows underprediction of surface and near-surface temperatures for the cold periods centered on DOY 365, 20, and 45. Simulated near-surface surface temperatures were almost  $5^\circ\text{C}$  too low for the period centered on DOY 45. We have no explanation for this large discrepancy.

#### 4.3 Components of the surface heat budget

Figure 4 shows daily averages of radiative and turbulent fluxes for the experiment. Recall that shortwave and incident longwave radiation were measured, while SNTHERMP computes the remaining fluxes. We display the turbulent fluxes with a sign change, so positive fluxes in all panels represent heat gained by the snow cover. We

compare these simulations with average daily measured fluxes from Persson et al. (2002), shown in their Fig. 20.

Because correct snow-surface temperature prediction is the main variant in our flux computation, measured and simulated fluxes track quite closely after 28 May (DOY 148), when the snow is melting and at  $0^\circ\text{C}$ . The following remarks mainly concern the pre-melt period.

The longwave radiation plot shows remarkably close agreement except during the following periods: 8 December 1997 to 3 January 1998 (DOY 342 to 8), 5 January to 25 January 1997 (DOY 5 to 15), and 6 February to 21 February (DOY 37 to 52). These periods correspond with those when SNTHERMP underpredicted surface temperature and in-snow near-surface temperatures (see Fig. 3). Low winds and low air temperatures prevailed during these periods.

The sensible heat plot also shows close agreement between measured and simulated fluxes. Predicted sensible heat fluxes, however, show overall too much surface heating in the winter and too much cooling in the spring. Peak warming episodes were sometimes too high by 25–50%. We looked more closely at predictions for the peaks occurring on 9 December, 21 February, and 6 March (DOY 343, 52, and 66). All cases shared high winds ( $8\text{--}10 \text{ m s}^{-1}$ ) and appeared to

follow the passage of synoptic fronts. While modeled and observed surface temperatures were usually within  $0.5^{\circ}\text{C}$ , modeled temperatures were consistently too low. Because of the high wind speeds, however, even this small discrepancy caused a significant error in the predicted flux.

Large cooling spikes on 9 December, 26 January, and 28 January (DOY 342, 26, and 28) were not captured by SNTHERMP. We have not investigated the cause of these discrepancies but note that wind speeds were mostly above  $10\text{ m s}^{-1}$  for these days.

SNTHERMP consistently overpredicted sensible heat cooling for the unstable period between 13 April and 21 May (DOY 103 through 141). Modeled surface temperatures were generally too high, frequently by  $1^{\circ}\text{C}$ .

Both measured and modeled latent heat fluxes were small ( $< 5\text{ W m}^{-2}$ ) during the winter. Before the onset of melt in the spring, modeled daily averages showed stronger surface cooling than the measurements.

## 5. ESTIMATING THE SENSIBLE HEAT FLUX WITH MODELS OF DIFFERING COMPLEXITY

Figures 5 through 7 compare the sensible heat flux  $H_s$  measured by eddy correlation on the ASFG tower and simulated by SNTHERMP. We compare three increasingly simplified formulations: a heterogeneous snowpack (standard SNTHERMP run), a homogenous snowpack, and a single-layer snowpack. We limit our analysis to the first of two winter aerodynamic regimes identified by Andreas et al. (2003b). During this period, from the start of the experiment on 31 October 1997 (day 304) through 14 May 1998 (day 134), the snow was dry and all the ice was snow covered.

Figure 5 shows high correlation between simulated and measured  $H_s$  for the standard SNTHERMP simulation. Although the correlation is about 0.9, the simulation overpredicts surface warming in stable stratification and shows considerable scatter in unstable stratification. The results for the stable case corroborate the trends shown in Fig. 4. Simulated outliers during unstable stratification mostly occurred between 8 May and 11 May (DOY 128 to 131) and coincided with diurnal solar warming of the snowpack.

Andreas et al. (2003b) note that disequilibrium in surface ice and air temperatures could also cause errors in predicted sensible heat. Ice temperatures slightly above and below the air temperature caused by respective radiational cooling

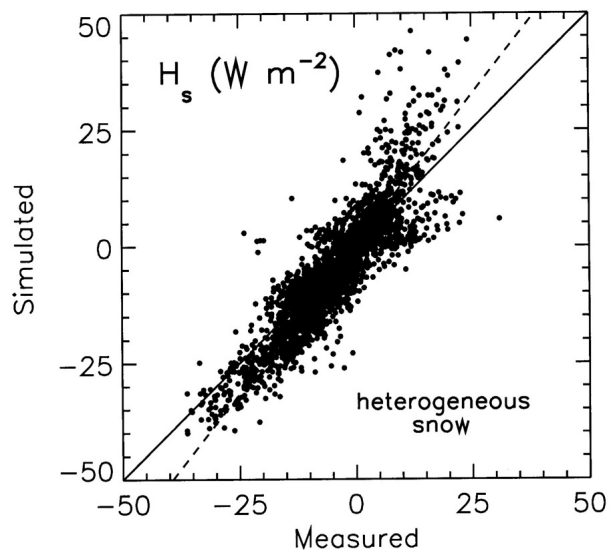


Fig. 5. Hourly averaged eddy-correlation measurements of the sensible heat flux,  $H_s$ , and the values simulated with SNTHERMP for a heterogeneous snow cover, the standard version of SNTHERMP. The solid line is 1:1; the dashed line is the best fit,  $\text{Sim} = 1.283\text{Meas} + 0.443$ . The correlation coefficient is 0.881.

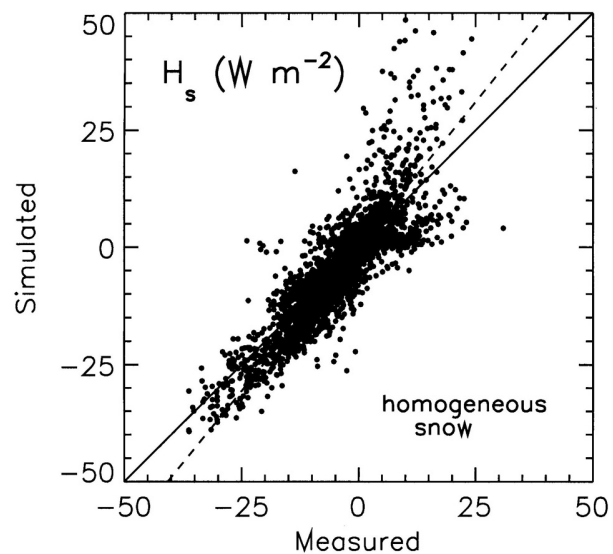


Fig. 6. As in Fig. 5 except the simulation is for a homogenous snow cover having a density of  $330\text{ kg m}^{-3}$ , a thermal conductivity of  $0.33\text{ W m}^{-1}\text{ K}^{-2}$ , but multiple snow layers, each with its own temperature. The best-fit line (dashed) is  $\text{Sim} = 1.232\text{Meas} + 0.204$ . The correlation coefficient is 0.861.

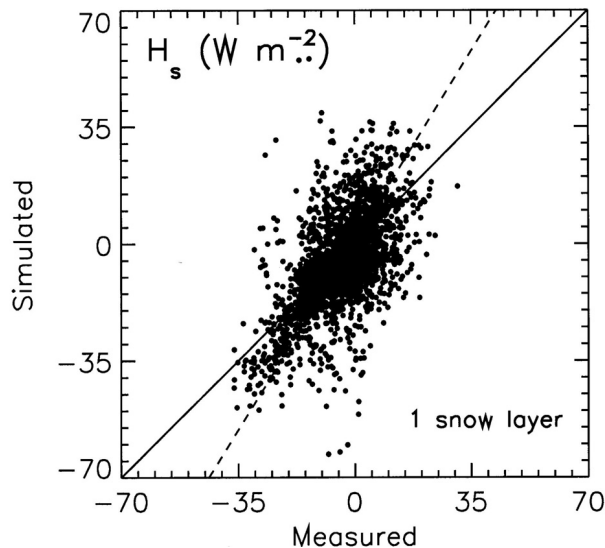


Fig. 7. As in Fig. 6 except the simulation has only one snow layer. The best-fit line (dashed) is  $\text{Sim} = 1.619\text{Meas} + 0.957$ . The correlation coefficient is 0.594.

and heating in stable and unstable conditions could explain part of the bias shown by Fig. 5.

Figure 6 is the same as for Fig. 5, except that for snow density and thermal conductivity we use constant values of  $330 \text{ kg m}^{-3}$  and  $0.33 \text{ W m}^{-1} \text{ K}^{-1}$ . We retain snow layers with different temperatures, though. This constant density value has long been used by sea ice modelers (e.g., Maykut and Untersteiner 1971, Ebert and Curry 1993), and Sturm et al. (2002a) inferred the average thermal conductivity value from snow temperature profiles at SHEBA. We adjusted precipitation so that simulated snow depths matched those for the standard simulation. The scatter plot for the homogenous simulation is almost identical to that for the heterogeneous snowpack. Considering the gain in model simplification, this is a very promising result.

Figure 7 is the same as for Fig. 6, except we use a single snow layer. SNTHERMP usually uses a body-centered nodal system. For this simulation, we use a “half” control volume for the snow layer, which places the top node at the snow surface. Figure 7 shows further degradation in prediction accuracy from Fig. 6. The largest simulation errors occur during rapid warming or cooling of the surface, when a thick, single layer cannot respond sufficiently fast to the forcing data (e.g., Guest and Davidson 1994).

## 6. CONCLUSIONS

For modeling the thin, wind-swept snow cover at SHEBA, we made several modifications to SNTHERMP to accumulate the correct snow cover and to capture the thermal exchange within the snow and at its surface. These include modifying the thermal conductivity of sea ice for air content, decreasing the precipitation enhancement factor at higher wind speeds, increasing new-snow density with decreasing temperature below  $-10^\circ\text{C}$ , and adding the convective transfer of heat through windpumping. We also increased the unit bond area in the Pitman and Zuckerman (1968) equation from 0.0071 to 0.012.

Our first simulations of the SHEBA data underpredicted cooling near the ice surface by several degrees. With the above adjustments, we were able to replicate the in-snow temperature traces fairly closely. Clearly, however, many questions remain about the exact mechanisms for heat transfer within the SHEBA snowpack. Questions also remain regarding mechanisms for densification and how to predict the new-snow density in the early snow of fall.

Simulated surface temperatures  $T_s$  were mostly within  $1^\circ\text{C}$  of our surface-based radiometric observations. Our estimates of the surface heat flux components, therefore, track fairly closely with observations. Because our estimates of  $T_s$  were biased low in the winter and high in the spring, both upwards and downwards peaks in simulated sensible heat fluxes to the surface were too large. Even small errors in  $T_s$  produced significant errors in the simulated sensible heat flux of up to 50% on very windy days.

A scatter plot of simulated versus eddy-correlation measurements of sensible heat flux is highly correlated (Fig. 5) but also shows a bias towards larger fluxes in the simulation. An alternative simulation with a constant snow density and thermal conductivity (Fig. 6) predicts the fluxes almost as well. A third simulation with a single snow layer (Fig. 7) shows considerably more scatter. These results suggest that assuming homogeneous snow is reasonable for GCM applications, but the snow cover must still be subdivided into several layers, each with its own temperature.

## 7. ACKNOWLEDGMENTS

The U.S. National Science Foundation supported this work with awards to CRREL,

NOAA/ETL, and NPS. The U.S. Department of the Army provided additional support to Andreas and Jordan through projects at CRREL.

## 8. REFERENCES

- Andreas, E. L., 1987: A theory for the scalar roughness and the scalar transfer coefficients over snow and sea ice. *Bound.-Layer Meteor.*, **38**, 159–184.
- \_\_\_\_\_, 2002: Parameterizing scalar transfer over snow and ice: A review. *J. Hydrometeor.*, **3**, 417–432.
- \_\_\_\_\_, C. W. Fairall, P. S. Guest, and P. O. G. Persson, 1999: An overview of the SHEBA atmospheric surface flux program. Preprints, *Fifth Conf. on Polar Meteorology and Oceanography*, Dallas, TX, Amer. Meteor. Soc., 411–416.
- \_\_\_\_\_, K. J. Claffey, C. W. Fairall, P. S. Guest, R. E. Jordan, and P. O. G. Persson, 2002: Evidence from the atmospheric surface layer that the von Kármán constant isn't. Preprints, *15th Symp. on Boundary Layers and Turbulence*, Wageningen, The Netherlands, Amer. Meteor. Soc., 418–421.
- \_\_\_\_\_, R. E. Jordan, and A. P. Makshtas, 2003a: Parameterizing turbulent exchange over sea ice: The Ice Station Weddell results. *J. Climate*, submitted.
- \_\_\_\_\_, R. E. Jordan, and A. P. Makshtas, 2003b: Simulations of snow, ice, and near-surface atmospheric processes on Ice Station Weddell. *J. Climate*, submitted.
- \_\_\_\_\_, C. W. Fairall, A. A. Grachev, P. S. Guest, T. W. Horst, R. E. Jordan, and P. O. G. Persson, 2003c: Turbulent transfer coefficients and roughness lengths over sea ice: The SHEBA results. Preprints, *Seventh Conf. on Polar Meteorology and Oceanography*, Hyannis, MA, Amer. Meteor. Soc., to appear.
- Colbeck, S., E. Akitaya, R. Armstrong, H. Gubler, J. Lafeuille, K. Lied, D. McClung, and E. Morris, Eds., 1990: *The International Classification for Seasonal Snow on the Ground*. International Glaciological Society, 23 pp.
- Crocker, G. B., 1984: A physical model for predicting the thermal conductivity of brine-wetted snow. *Cold Reg. Sci. Technol.*, **10**, 69–74.
- Cunningham, J., and E. D. Waddington, 1993: Air flow and dry deposition of non-sea salt sulfate in polar firn: Paleoclimatic implications. *Atmos. Environ.*, **27A**, 2943–2956.
- Ebert, E. E., and J. A. Curry, 1993: An intermediate one-dimensional thermodynamic sea ice model for investigating ice-atmosphere interactions. *J. Geophys. Res.*, **98**, 10,085–10,109.
- Goodison, B. E., and D. Yang, 1996: In-situ measurements of solid precipitation in high latitudes: The need for correction. Presented at Workshop on the ACSYS Solid Precipitation Climatology Project, World Meteor. Org., Geneva.
- Guest, P.S., and K.L. Davidson, 1994: Factors affecting variations of snow surface temperature and air temperature over sea ice in winter. *The Polar Oceans and Their Role in Shaping the Global Environment*, Nansen Centennial Volume, O. M. Johannessen, R. D. Muench and J. E. Overland, eds., American Geophysical Union, Washington DC, 435–442.
- Holtslag, A. A. M., and H. A. R. DeBruin, 1988: Applied modeling of the nighttime surface energy balance over land. *J. Appl. Meteor.*, **27**, 689–704.
- Jordan, R. E., 1991: A one-dimensional temperature model for a snow cover: Technical documentation for SNTHERM.89. Spec. Rep. 91–16, U.S. Army Cold Regions Research and Engineering Laboratory, Hanover, NH, 49 pp.
- \_\_\_\_\_, E. L. Andreas, and A. P. Makshtas, 1999: Heat budget of snow-covered sea ice at North Pole 4. *J. Geophys. Res.*, **104**, 7785–7806.
- \_\_\_\_\_, E. L. Andreas, and A. P. Makshtas, 2001: Modeling the surface energy budget and the temperature structure of snow and brine-snow at Ice Station Weddell. Preprints, *Sixth Conf. on Polar Meteorology and Oceanography*, San Diego, CA, Amer. Meteor. Soc., 129–132.
- Kharitonov, G. G., 1974: Physical properties of new snow and related meteorological factors (in Russian). Toshkent, Cent. Reg. Sci. Res. Hydrometeo Inst., Trudy, **15**, 94–106.
- Maykut, G. A., and N. Untersteiner, 1971: Some results from a time dependent thermodynamic model of sea ice. *J. Geophys. Res.*, **76**, 1550–1575.
- Morris, E. M., H.-P. Bader, and P. Weilenmann, 1997: Modelling temperature variations in polar snow using DAISY. *J. Glaciol.*, **43**, 180–191.

- Paulson, C. A., 1970: The mathematical representation of wind speed and temperature profiles in the unstable atmospheric surface layer. *J. Appl. Meteor.*, **9**, 857–861.
- Perovich, D. K., and B. Elder, 2001: Temporal evolution and spatial variability of the temperature of Arctic sea ice. *Ann. Glaciol.*, **33**, 207–211.
- Perovich, D. K., T. C. Grenfell, B. Light, J. A. Richter-Menge, M. Sturm, W. B. Tucker III, H. Eicken, G. A. Maykut, and B. Elder, 1999: SHEBA: Snow and Ice Studies [CD-ROM]. U.S. Army Cold Regions Research and Engineering Laboratory, Hanover, NH.
- Perovich, D. K., T. C. Grenfell, J. A. Richter-Menge, B. Light, W. B. Tucker III, and H. Eicken, 2003: SHEBA: Thin and thinner: Sea ice mass balance measurements during SHEBA. *J. Geophys. Res.*, **108**, DOI: 10.1029/2001JC001079, in press.
- Persson, P. O. G., C. W. Fairall, E. L. Andreas, P. S. Guest, and D. K. Perovich, 2002: Measurements near the Atmospheric Surface Flux Group tower at SHEBA: Near-surface conditions and surface energy budget. *J. Geophys. Res.*, **107** (C10), DOI: 10.1029/2000JC000705.
- Pitman, D., and B. Zuckerman, 1968: Effective thermal conductivity of snow at  $-88^{\circ}\text{C}$ ,  $-27^{\circ}\text{C}$ , and  $-5^{\circ}\text{C}$ . *Research in Space Science*, Spec. Rep. 267, Smithsonian Institution Astrophysical Observatory, Cambridge, MA, 23 pp.
- Rowe, C. M., K. C. Kuivinen, and R. Jordan, 1995: Simulation of summer snowmelt on the Greenland ice sheet using a one-dimensional model. *J. Geophys. Res.*, **100**, 16,265–16,273.
- Schwerdtfeger, P., 1963: The thermal properties of sea ice. *J. Glaciol.*, **4**, 789–807.
- Sturm, M., 1991: The role of thermal convection in heat and mass transport in the subarctic snow cover. CRREL Rep. 91–19, U.S. Army Cold Regions Research and Engineering Laboratory, Hanover, NH, 84 pp.
- Sturm, M., J. Holmgren, M. König, and K. Morris, 1997: The thermal conductivity of seasonal snow. *J. Glaciol.*, **43**, 26–41.
- Sturm, M., D. K. Perovich, and J. Holmgren, 2002a: Thermal conductivity and heat transfer through the snow on the ice of the Beaufort Sea. *J. Geophys. Res.*, **107** (C10), DOI:10.1029/2000JC000466.
- Sturm, M., J. Holmgren, and D. K. Perovich, 2002b: Winter snow cover on the sea ice of the Arctic Ocean at the Surface Heat Budget of the Arctic Ocean (SHEBA): Temporal evolution and spatial variability. *J. Geophys. Res.*, **107** (C10), DOI:10.1029/2000JC000400.
- Yen, Y. C., 1965: Effective thermal conductivity and water diffusivity of naturally compacted snow. *J. Geophys. Res.*, **70**, 1821–1825.